Title: High metabolism and periodic hypoxia associated with drifting macrophyte detritus in the shallow subtidal Baltic Sea

Author list: Karl M. Attard[1,2,3], Anna Lyssenko[3], Iván F. Rodil[3,4]

Corresponding author: Karl M. Attard karl.attard@biology.sdu.dk

Author affiliations:

[1] Department of Biology, University of Southern Denmark, 5230 Odense M, Denmark

[2] Danish Institute for Advanced Study, University of Southern Denmark, 5230 Odense M, Denmark

[3] Tvärminne Zoological Station, University of Helsinki, J.A. Palménin tie 260, 10900 Hanko, Finland

[4] Department of Biology (INMAR), Faculty of Marine and Environmental Sciences, University of Cádiz, Puerto Real, Spain

Keywords: benthic ecosystems, primary production, respiration, oxygen fluxes, biodiversity

Abstract

Macrophytes form highly productive habitats that export a substantial proportion of their primary production as particulate organic matter. As the detritus drifts with currents and accumulates in seafloor depressions, it constitutes organic enrichment and can deteriorate O_2 conditions on the seafloor. In this study, we investigate the O_2 dynamics and macrobenthic biodiversity associated with a shallow ~2300 m^2 macrophyte detritus field in the northern Baltic Sea. The detritus, primarily *Fucus vesiculosus* fragments, had a biomass of ~1700 g dry weight m^{-2}, approximately 1.5-fold larger than nearby intact *F. vesiculosus* canopies. A vertical array of O_2 sensors placed within the detritus documented that hypoxia ($[O_2] < 63$ µmol L^{-1}) occurred for 23% of the time and terminated at the onset of wave-driven hydrodynamic mixing. Measurements in five other habitats nearby spanning bare sediments, seagrass, and macroalgae indicate that hypoxic conditions were unique to detritus canopies. Fast-response O_2 sensors placed above the detritus documented pulses of hypoxic waters originating from within the canopy. These pulses triggered a rapid short-term (~5 min) deterioration of O_2 conditions within the water column. Eddy covariance measurements of O_2 fluxes indicated high metabolic rates with daily photosynthetic production offsetting up to 81 % of the respiratory demands of the detritus canopy, prolonging its persistence within the coastal zone.

29   The detritus site had a low abundance of crustaceans, bivalves, and polychaetes when compared to

30   other habitats nearby, likely because their low-O_2 tolerance thresholds were often exceeded.

31   **1. Introduction**

32   Oxygen availability determines ecosystem health and the biogeochemical function of coastal waters

33   (Diaz and Rosenberg, 2008; Middelburg and Levin, 2009; Breitburg et al., 2018). When in gaseous

34   equilibrium with air, seawater typically contains an O_2 concentration ($[O_2]$) between 200-400 µmol

35   L^{-1}, depending on the water temperature and the salinity (Garcia and Gordon, 1992). However, both

36   abiotic and biotic processes cause significant departures from equilibrium. The main source of O_2 to

37   coastal waters is the atmosphere, where the diffusion of O_2 is governed by the air-to-sea gas

38   exchange rate (Berg and Pace, 2017; Long and Nicholson, 2018). In shallow waters and light-

39   exposed seafloor sediments, O_2 is produced by primary producers as a by-product of

40   photosynthesis, and it is consumed by consortia of microbes and fauna directly, through aerobic

41   respiration, and indirectly, through the oxidation of reduced substances (Glud, 2008). If O_2

42   consumption exceeds supply for a sufficiently long period, O_2 conditions deteriorate and become

43   hypoxic ($[O_2] < 63$ µmol L^{-1}). Hypoxia is becoming more common, more intense, and is affecting

44   larger areas of coastal waters, increasingly placing ecosystems and the services they provide at risk

45   (Breitburg et al., 2018). There are several well-known variants of coastal hypoxia (Diaz and

46   Rosenberg, 2008; Carstensen and Conley, 2019). Seasonal hypoxia, the most common form,

47   typically occurs in summer when warm waters, strong stratification, and high organic enrichment

48   combine to deplete O_2 until autumn (Robertson et al., 2016). Periodic hypoxia, in contrast, occurs

49   more often due to local weather dynamics and tidal cycles but individual events are shorter (Diaz

50   and Rosenberg, 1995), whereas diel cycles with large day-to-night $[O_2]$ excursions trigger hypoxia

51   for a few hours daily (Davanzo and Kremer, 1994; Tyler et al., 2009). All events are expected to

52   affect biodiversity and biogeochemical cycling to varying degrees. Seasonal and periodic hypoxia

53   are associated with large-scale mortality of organisms and a switch between retention and removal

54   of bioavailable nutrients such as nitrate, ammonium, phosphate, and toxic hydrogen sulfide

55   (Middelburg and Levin, 2009; Carstensen and Conley, 2019). Short-term hypoxia can similarly

56   exceed lethal and non-lethal thresholds for many taxa (Vaquer-Sunyer and Duarte, 2008), although,

57   due to their sporadic nature, their occurrence and impacts are less understood.

58   Given the importance of O_2 in coastal waters, $[O_2]$ is one of the most frequently measured

59   environmental parameters. Near-seabed $[O_2]$ is typically measured using long-term stable O_2

sensors (e.g. optodes) (Bittig et al., 2018) that are moored ~0.3-1.0 m above the seafloor, or by performing vertical profiles of water column $[O_2]$ down to ~1.0 m above the seafloor using multiparameter sondes. National monitoring programs such as those maintained by the Swedish Meteorological and Hydrological Institute and the Finnish Environment Institute provide a wealth of essential open-access data, enabling important analyses detailing the prevalence and intensity of coastal hypoxia (Virtanen et al., 2019; Conley et al., 2011; Carstensen and Conley, 2019). Notwithstanding the progress being made in coastal monitoring, it was demonstrated more than 40 years ago that the largest $[O_2]$ gradients may occur just a few cm above the seafloor due to the high reactivity of marine sediments and a strong benthic O_2 demand (Jorgensen, 1980). To date, records of hypoxia in the shallow subtidal zone are still somewhat scarce. In a compilation of monitoring data for the northern Baltic Sea (Gulf of Finland and Archipelago Sea), Virtanen et al. (2019) found that just 11 out of 461 (or 2.4%) of the monitoring stations that registered hypoxia occurred in waters < 5 m depth. While this may reflect a true signal that hypoxia is more widespread in deeper coastal waters, it is also likely that hypoxic conditions go undetected if measurements are performed away from the seafloor, as is common practice (Conley et al., 2011; Virtanen et al., 2019).

Around two-thirds of the ocean's photosynthetic biomass is bound in macrophytes growing in shallow waters along the world's coastline (Smith, 1981). Through seasonal decay, epiphyte growth, grazing, and physical forcing (e.g. waves, currents, ice scouring), macrophytes export a large proportion of their primary production (~40 %) to their surroundings as detritus (Attard et al., 2019a; Krumhansl and Scheibling, 2012; Duarte and Cebrián, 1996). Macrophyte detritus drifts with the currents and accumulates on the shoreline and in low-energy marine environments (e.g. shallow seafloor depressions and in deeper waters), where it constitutes habitat structure and organic enrichment to the receiving habitat (Norkko and Bonsdorff, 1996b). Given high enough abundance, detritus suppresses the diffusion of O_2 from the water column to the sediment surface and it exacerbates O_2 depletion on the seabed as it decays. Large accumulations of unattached ephemeral macroalgae such as the brown algae *Ectocarpus siliculosus* and *Pylaiella littoralis* are common in eutrophic coastal waters such as the Baltic Sea, forming thin mats above the seafloor typically a few centimeters thick (Norkko and Bonsdorff, 1996a). While coastal hypoxia is most commonly associated with eutrophic waters such as the Baltic Sea (Carstensen and Conley, 2019; Conley et al., 2011), hypoxic (and even sulfidic) conditions have been reported in remote and more pristine environments such as the high Arctic due to large accumulations of detritus produced from

perennial brown seaweeds (Glud et al., 2004). However, the O_2 dynamics within accumulations of drifting detritus and the potential implications for the associated fauna remain poorly understood. Understanding the ecological and biogeochemical implications of drifting macrophyte detritus is particularly important given the ambitions to vastly increase macroalgal farming (Broch et al., 2019), which would result in increased deposition of macrophyte detritus on the coastal seafloor (Broch et al., 2022).

In this study, we investigate the O_2 dynamics and macrobenthic biodiversity associated with a shallow ~2300 m^2 macrophyte detritus field composed of *Fucus vesiculosus* fragments in the northern Baltic Sea. To assess O_2 production versus consumption rates of the detritus canopy, we deployed an eddy covariance system on multiple occasions to extract benthic O_2 fluxes non-invasively. Using a vertical array of O_2 sensors and an acoustic velocimeter, we monitored O_2 distribution within the canopy and the hydrodynamics above the canopy to assess the occurrence and intensity of hypoxic events and their links to local hydrodynamics. We performed biodiversity surveys to identify the prevailing taxa, and we compared hypoxic thresholds of these taxa to [O_2] measured *in situ* to identify potential stress. Measurements were also performed in five other habitats nearby spanning bare sediments, seagrass, and macroalgae for comparison.

2. Materials and Methods

2.1. Study location

The study was performed in the microtidal Baltic Sea nearby the Tvärminne Zoological Station in SW Finland. Although the focus of our study was to investigate drifting macrophyte detritus, we selected an additional five study sites within the shallow subtidal zone (2-4 m depth) for comparison, representing key habitats in the Baltic Sea: one site with bare sediments, two sites with seagrass (predominantly *Zostera marina*; sheltered and exposed), and two sites with intact macroalgae canopies (predominantly *Fucus vesiculosus*; sheltered and exposed) (Table 1).

Site	Location	Deployment start	Deployment duration (h)	Water depth (m)	Water temperature (°C)	Minimum O_2 (µmol L^{-1})	Maximum O_2 (µmol L^{-1})	Hypoxia duration (h)
Macrophyte detritus	59 811613 N 23 206624 E	29-05-2018	120	3.0	12	0.6	429	27
Bare sediments	59 841532 N 23 253370 E	20-05-2018	96	3.7	11	307	407	0
Sheltered *Z. marina*	59 841551 N 23 251203 E	27-05-2018	87	4.0	16	272	333	0

Exposed *Z. marina*	59 827008 N 23 151976 E	08-06-2018	120	2.9	10	281	437	0
Sheltered *F. vesiculosus*	59 826856 N 23 209721 E	08-06-2018	120	2.0	10	253	489	0
Exposed *F. vesiculosus*	59 811359 N 23 207281 E	31-05-2018	116	2.0	9	287	427	0

116 Table 1: Environmental conditions and low-oxygen events at the six study sites

117

2.2. [O₂] dynamics in benthic habitats

119 To investigate the near-bed [O$_2$] dynamics and its environmental controls, we equipped a tripod
120 frame with a suite of sensors consisting of three cross-calibrated dissolved [O$_2$] loggers with inbuilt
121 temperature compensation (HOBO U26-001, Onset), a 6 MHz acoustic velocimeter (Vector,
122 Nortek), a photosynthetic active radiation (PAR) sensor (RBRsolo with Licor PAR Quantum
123 192SA), and a saltwater conductivity sensor (HOBO U24-002-C). The [O$_2$] loggers have a factory-
124 specified accuracy of $\pm$ 6 μmol L^{-1} from 0 to 250 μmol L^{-1}, $\pm$ 16 μmol L^{-1} from 250-625 μmol L^{-1}, a
125 resolution of 0.6 μmol L^{-1} and a 90% response time (T$_{90}$) < 2 min. The [O$_2$] and conductivity
126 sensors were mounted onto a 75 cm-long stainless-steel rail affixed to the tripod leg (Fig. 1). The
127 sensors were secured to the rail at various heights above the seabed using rail mount clamps. For the
128 study sites with canopies, two sensors were set inside the canopy; one sensor was ~5 cm above the
129 seafloor and one was close to the top of the canopy (15-25 cm). The third sensor was placed in the
130 water above the canopy (~35 cm above the seafloor). The tripod was deployed by divers from a
131 small boat and was carefully positioned on the seafloor using a lift bag. The exact sensor heights
132 were noted by the divers once the instrument was on the seafloor. The instrument was left to record
133 data for 3-5 days at each site. The velocimeter sampled three-dimensional flow velocity
134 continuously at 8 Hz, whereas the [O$_2$], temperature, conductivity, and PAR sensors recorded data
135 every minute.

136 To investigate [O$_2$] dynamics and its environmental drivers, all sensor time series were aligned in
137 time and analyses were performed to investigate vertical gradients in O$_2$ distribution, diel [O$_2$]
138 excursions, and boundary-layer hydrodynamics. We assessed the occurrence of hypoxia ([O$_2$] < 63
139 μmol L^{-1}) by quantifying the magnitude (lowest [O$_2$] value) and the duration (in hours) of hypoxic
140 events. The high-frequency velocity data were used to calculate mean flow velocity magnitude ($\bar{U}$)
141 as the sum of streamwise (u) and traverse (v) components, as $\bar{U} = \sqrt{u^2 + v^2}$.
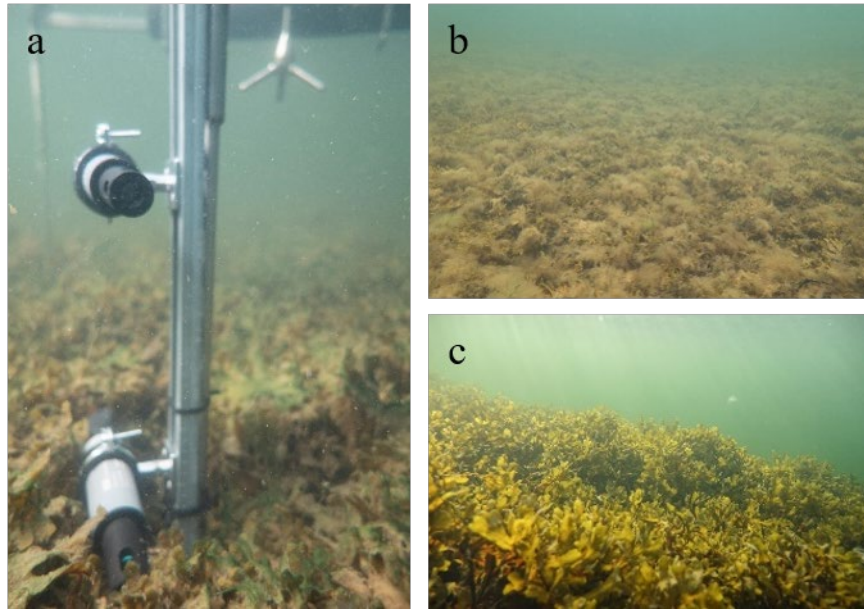
142

143   Fig. 1: The study area showing (a) the instrument deployed within the detritus canopy, (b) a broad-

144   scale view of the detritus accumulation area, and (c) a nearby intact *Fucus vesiculosus* canopy.

145   *2.3. Benthic O_2 fluxes*

146   An aquatic eddy covariance system was deployed at the detritus site to quantify benthic O_2 fluxes at

147   the canopy-water interface on three occasions (June 2017, September 2017, and May 2018). Eddy

148   covariance integrates over a relatively large seafloor area (typically ~30 m^2) (Berg et al., 2007), and

149   extracts fluxes without disturbing the hydrodynamics or the light, which is particularly useful when

150   trying to understand the mechanistic drivers of [O_2] dynamics (Berg et al., 2022). The eddy

151   covariance setup was identical to the tripod frame described above, with the addition of a fast-

152   response ($T_{90} < 0.3$ s) [O_2] microsensor setup for covariance measurements (McGinnis et al., 2011).

153   The hardware and data processing techniques are described in detail in Attard et al. (2019b). This

154   instrument can capture the entire range of flux-contributing turbulent eddies within the benthic

155   boundary layer, and this information is used to approximate the benthic O_2 flux non-invasively

156   (Berg et al., 2003; Berg et al., 2022). The instrument recorded co-located measurements of the

157   vertical velocity (*w*) and the O_2 concentration (*C*) at 32 Hz, and the data were processed using a

158   multiple-step protocol detailed in Attard et al. (2019b) to extract and quality-check benthic fluxes.

159   In short, the data streams for *w* and *C* were decomposed into mean and fluctuating components

160   using Reynolds decomposition, as $w = \bar{w} + w'$ and $C = \bar{C} + C'$ (Berg et al., 2003). The turbulent

161   flux (J_{EC}) was then computed in units of mmol O_2 m^{-2} h^{-1} as $J_{EC} = \overline{w'C'}$, where the overbar

162 represents a period of 15 min. The turbulent flux was then summed with a storage correction term to

163 calculate the total benthic flux ($J_{benthic}$, mmol O_2 m^{-2} h^{-1}) (Rheuban et al., 2014), as:

$$J_{benthic} = J_{EC} + \int_0^h \frac{\partial C}{\partial t}\, \mathrm{d}z$$

165 The storage correction term was defined using the three [O_2] optodes placed within and above the

166 canopy. For the correction, we defined a matrix with the number of rows n corresponding to the

167 sensor measurement height above the seafloor (1 row per cm) (Camillini et al., 2021). To do this,

168 the oxygen time series, consisting of [O_2] measurements performed at three heights within the

169 canopy, were converted to a matrix using the software package OriginPro 2022. Since the

170 measurement height of the three sensors were spaced nonlinearly, the data were first converted to

171 XYZ column format using the w2xyz function. Next, the three rows, representing the [O_2] time

172 series measurements at three heights, were expanded to n rows, with n representing the sensor

173 measurement height in cm (from 0 to n cm above seabed, 1 row per cm) using the XYZ Gridding

174 function. This generated a matrix of n rows consisting of linearly interpolated [O_2]. Interpolation

175 was performed using the Random (Renka Cline) gridding method. Next, a storage correction term

176 was calculated for each 1 cm cell as described by Rheuban et al. (2014), and the total storage

177 correction was subsequently computed for the water volume below the sensor measurement height

178 as the sum of the n rows. The high-frequency [O_2] time series from the fast-response microsensors

179 were also analyzed to identify any pulses of low [O_2] waters originating from within the canopy and

180 propagating upwards into the water column.

181 *2.4. Benthic metabolic rates*

182 The O_2 flux time series was separated into individual 24 h periods (midnight to midnight). The

183 daytime flux (Flux$_{day}$, mmol O_2 m^{-2} h^{-1}) was computed as a bulk average of fluxes measured when

184 PAR > 1.0 μmol m^{-2} s^{-1}. The nighttime flux (Flux$_{night}$, mmol O_2 m^{-2} h^{-1}) was calculated as the

185 average of the remaining fluxes, when PAR < 1.0 μmol m^{-2} s^{-1}. These two values and the number of

186 daylight hours (h_{day}) were used to estimate the daily photosynthetic rate, termed the gross primary

187 production (*GPP*, in mmol O_2 m^{-2} d^{-1}), as $GPP = Flux_{day} + abs(Flux_{night}) * h_{day}$, and daily

188 respiration (*R*, in mmol O_2 m^{-2} d^{-1}), as $R = abs(Flux_{night}) * 24$, assuming a light-independent

189 respiration rate. The latter is a common assumption, but it is known that it underestimates the true

190 metabolic activity (Fenchel and Glud, 2000; Juska and Berg, 2022). The daily balance between

191   *GPP* and *R*, termed the net ecosystem metabolism (*NEM*, in mmol O_2 m^{-2} d^{-1}) was estimated as

192      $NEM = GPP - R$ (Attard et al., 2019b).

193   The relationship between seafloor PAR and the in situ benthic O_2 flux was investigated using light-

194   saturation curves. Hourly O_2 fluxes were plotted against the corresponding near-bed incident PAR

195   and the relationship between the two was investigated using a modified tangential hyperbolic

196   function by Platt et al. (1980), as $O_2\ flux = P_m * \tanh\left(\frac{\alpha I}{P_m}\right) - R$, where P_m is the maximum rate of

197   hourly gross primary production, α is the initial quasi-linear increase in O_2 flux with PAR, I is near-

198   bed irradiance (PAR), and R is the dark respiration rate. The photosaturation parameter, I_k (μmol

199   PAR m^{-2} s^{-1}) was derived as P_m/α. Non-linear curve fitting was performed in OriginPro 2022 using

200   a Levenberg–Marquardt iteration algorithm, until a Chi-Squared tolerance value of 1E-9 was

201   reached (Attard and Glud, 2020).

202   *2.5. Biodiversity sampling*

203   At all six sites, we aimed to obtain a quantitative understanding of the abundance, biomass, and

204   species richness of macrophytes and macrofauna (infauna and epifauna). The different habitats

205   required different sampling strategies, since four sites were sedimentary (bare sediments site, two

206   seagrass sites, and the detritus sites) and two sites were rocky (two macroalgal sites) (Rodil et al.,

207   2019).

208   At the time of our study, the detritus site had a ~20-cm thick detritus mat covering the seabed

209   sediments. The detritus canopy was sampled using large stainless steel core liners (inner diameter =

210   19 cm; $n = 4$) capable of cutting through the mat, and the collected samples were transferred into a

211   fine-mesh bag. In the laboratory, the detritus was rinsed through a 0.5 mm sieve to collect the

212   associated epifauna. Samples of algal detritus were dried at 60°C for 48 hours and the biomass was

213   calculated as dry weight /m^2.

214   Macroinfauna at the four sedimentary habitats was sampled using six sediment cores (inner

215   diameter = 5.0 cm, depth = 15 cm). The samples were sieved through a 0.5 mm sieve and animals

216   were stored in alcohol for later identification. At the seagrass sites, representative macrophyte

217   samples were collected by divers from an area around the tripod frame at the end of the deployment

218   using four randomly-placed quadrats (20 x 20 cm). The seagrass within each quadrat was gently

219   uprooted and was transferred into a net-bag. In the laboratory, the samples were rinsed through a

220   0.5 mm sieve to collect all the associated epifauna. The animals were stored in alcohol for later

identification, and the seagrass was frozen in sealed bags for further processing. The seagrass samples were later thawed, and individual shoots were counted to determine the canopy density in m^2. The above- and below-ground macrophyte biomass was separated, dried at 60°C for 48 hours and weighed.

At the rocky sites, *F. vesiculosus* individuals ($n = 4$) were randomly collected from around the instrument in fine-mesh bags. Randomly-placed quadrats (1 m^2, $n = 4$) were used to quantify the number of *F. vesiculosus* individuals per m^2. At the laboratory, the collected *F. vesiculosus* samples were carefully rinsed through a 0.5 mm sieve to collect the epifauna. The height of the *F. vesiculosus* canopy was determined from the average length of the sampled individuals. Both *F. vesiculosus* and epiphytes were separated to the extent possible, dried at 60 °C for 48 h and weighed. To collect any macrofauna on the bare rock beneath the *F. vesiculosus* canopy, Kautsky-type samplers were placed on the seafloor and the 20 cm x 20 cm area was gently scraped using a spoon into a fine-mesh sampling bag. In the laboratory, all the macrofauna from the four replicates were sieved through a 0.5 mm sieve and stored in alcohol.

The fauna from all habitats was sorted, identified to species level, counted, and weighed. The wet weight for each species was noted with 0.0001 g accuracy. In cases where the fauna occurred in very high numbers, the sample was placed in a water-filled tray and divided into eight sectors. Four sectors were randomly chosen to calculate abundance and biomass. The length of gastropods and bivalves was measured from anterior to posterior axis using Vernier callipers (accuracy = 0.01 mm) for conversion to ash-free dry mass (AFDM). The AFDM of bivalves and gastropods was calculated using established relationships between length and weight for Baltic Sea fauna (Rumohr et al., 1987).

The abundance (ind m^{-2}) and biomass (AFDM/SFDM g m^{-2}) of the invertebrates across sites were calculated. Primer (v.7 and PERMANOVA+) software was used to perform the nonmetric multidimensional scaling (nMDS, with fourth-root-transformed data) to visualize macrofauna assemblages between sites. ANOSIM based on the Bray-Curtis similarity matrix was also performed in Primer (site as a fixed factor, 4999 random sample permutations) to compare differences in macrofauna abundance and biomass between sites.

3. Results

3.1. Environmental conditions

252   Average water depth ranged from 2.0 m to 4.0 m at the six study sites, and average water

253   temperature ranged from 9 °C to 16 °C during the study period (Table 1). Hypoxic conditions were

254   only detected at the detritus site. Bottom-water [O_2] at the detritus site ranged from 1 µmol L^{-1} to

255   429 µmol L^{-1}, with hypoxic conditions occurring for 27 h out of the 120 h long deployment (i.e. for

256   23 % of the time) (Table 1). At the five other measurement sites, [O_2] were well above hypoxic

257   conditions, with overall concentrations following diel patterns and ranging from 250 µmol L^{-1} to

258   490 µmol L^{-1} (Table 1).

259   *3.2. [O_2] dynamics in detritus canopies*

260   The [O_2] measurements within the detrital canopy document a highly dynamic [O_2] environment

261   driven by light availability and flow velocity (Fig. 2). Within the upper layers of the canopy (i.e.

262   ~10 to 25 cm above the seafloor), [O_2] and temporal dynamics largely follow diel patterns driven by

263   light availability, with large ~250 µmol L^{-1} diel excursions in [O_2]. There, the [O_2] was lowest in

264   the morning (~160 µmol L^{-1}) and highest in the evening (~430 µmol L^{-1}). In all cases, [O_2] within

265   the upper canopy region was above hypoxic thresholds. However, under low average flow

266   velocities < 2 cm s^{-1}, [O_2] within the lower canopy region (< 10 cm) deviated substantially from the

267   conditions above. No diel variations in [O_2] were observed during these periods, and [O_2] rapidly

268   became hypoxic for sustained periods (> 24 h long), with [O_2] being very low (< 10 µmol L^{-1})

269   during ~10 hr (~8 % of the time) (Fig. 2). As hypoxia persisted throughout the night under low flow

270   velocities, low [O_2] extended upwards into the canopy. Hypoxic conditions ended at the onset of

271   higher mean flow velocities of ~7 cm s^{-1}, which initiated a rapid (i.e. within 1.5 hr) oxygenation of

272   the entire canopy.

273
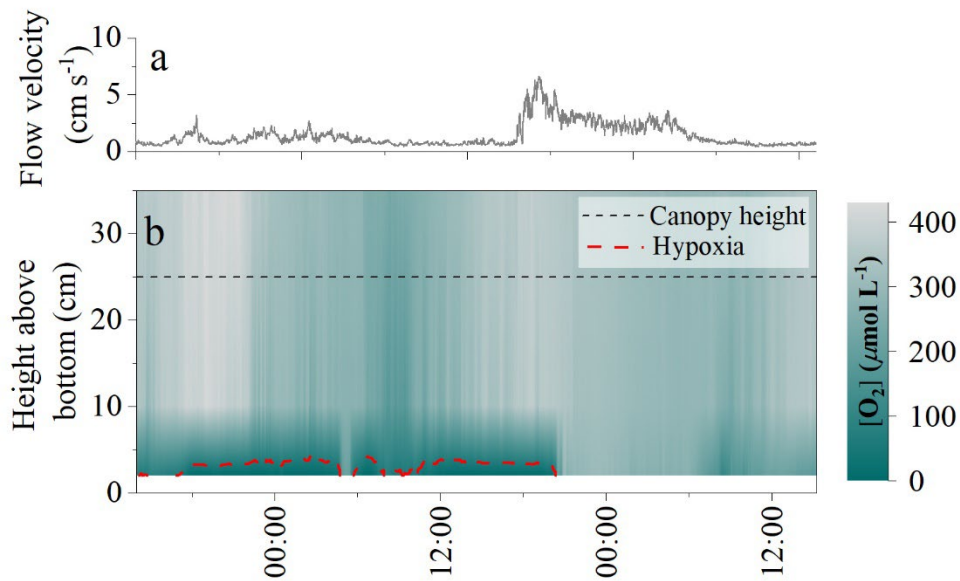
Fig. 2: (a) Flow velocity measured by the velocimeter 10 cm above the detritus canopy and (b) O_2 distribution within the canopy as resolved by three O_2 sensors located at 3 cm, 10 cm, and 35 cm above the seafloor. Deployment starting from 29th May 2018.

3.3. Pulses of hypoxic waters

High-frequency [O_2] measurements performed 10 cm above the detritus canopy document transient pulses of hypoxic water originating from within the canopy and propagating upwards into the water column (Fig 3). Such pulses typically followed quiescent weather and occurred at the onset of increased flow velocities. It took < 1 min to reduce [O_2] in the water column from 220 µmol L^{-1} to 65 µmol L^{-1}. Subsequently, a recovery period followed where [O_2] gradually increased back to previous concentrations over a ~5 min period. These rapid variations in water column [O_2] were not captured by the slow-response [O_2] optode sampling at 1 min intervals.
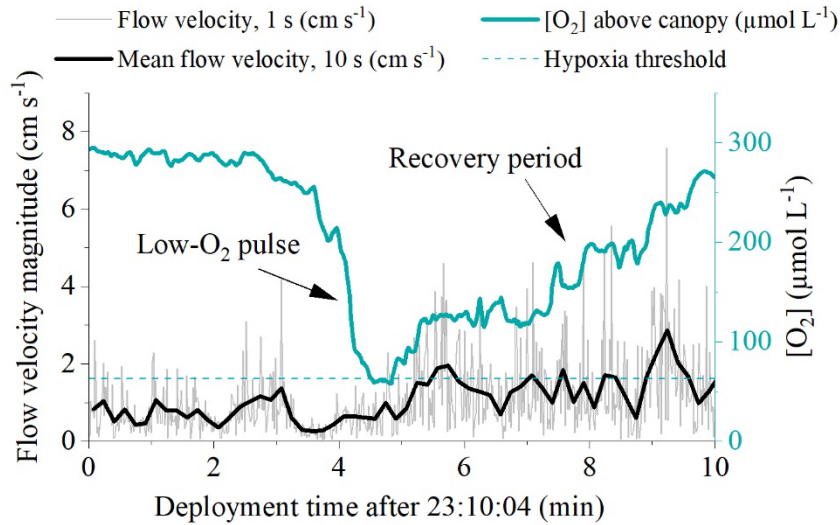
Figure 3: High-frequency $[O_2]$ measured 10 cm above the detrital canopy documented pulses of hypoxic water originating from within the canopy and propagating upwards into the water column. Data from 20th September 2017.

3.4. Benthic O_2 fluxes and detritus metabolic rates

The eddy covariance measurements at the detritus site produced three days of continuous flux data in June 2017, three days of data in September 2017, and five days of data in May 2018. Benthic O_2 fluxes documented a dynamic O_2 exchange rate driven by light availability and flow velocity. During quiescent periods with low flow velocity < 2 cm s^{-1}, a clear diel signal in the O_2 flux was observed, indicating substantial primary production associated to the detritus canopy. Higher flow velocities stimulated O_2 uptake rates by up to 5-fold, indicating that canopy ventilation through mixing increased O_2 uptake.

Hourly O_2 fluxes ranged from -22 mmol O_2 m^{-2} h^{-1} at night to 13 mmol O_2 m^{-2} h^{-1} during the day and showed a distinct diel cycle in response to sunlight availability (Fig. 4). Daily R ranged from 26 to 97 mmol O_2 m^{-2} d^{-1}, and daily GPP was between 15 and 74 mmol O_2 m^{-2} d^{-1}. Daily R exceeded GPP in all 11 measurement days (net heterotrophic), with NEM ranging from -7 to -32 mmol O_2 m^{-2} d^{-1} (Fig. 4, Table A1). The deployment average (± SD) GPP:R for the detritus canopy was 0.77 ± 0.04 in June 2017 (*n* = 3), 0.55 ± 0.02 in September 2017 (*n* = 3), and 0.77 ± 0.00 in May 2018 (*n* = 5), and the global mean GPP:R was 0.71 ± 0.11 (n = 11).

There was a significant positive relationship between daily detritus GPP and R in all measurement campaigns, with the detritus canopy seemingly becoming more heterotrophic (i.e. R > GPP) as the

magnitude of the metabolic rates increased (Fig. 5, Table A1). Significant positive relationships

were also observed between daily detritus GPP and daily seabed PAR (Table A1). Canopy light-use

efficiency (LUE), estimated as the ratio between daily GPP and daily PAR (Attard and Glud, 2020),

was 0.004 O_2 photon^{-1} in June 2017, 0.006 O_2 photon^{-1} in September 2017, and 0.004 O_2 photon^{-1} in

May 2018 (Table A1).
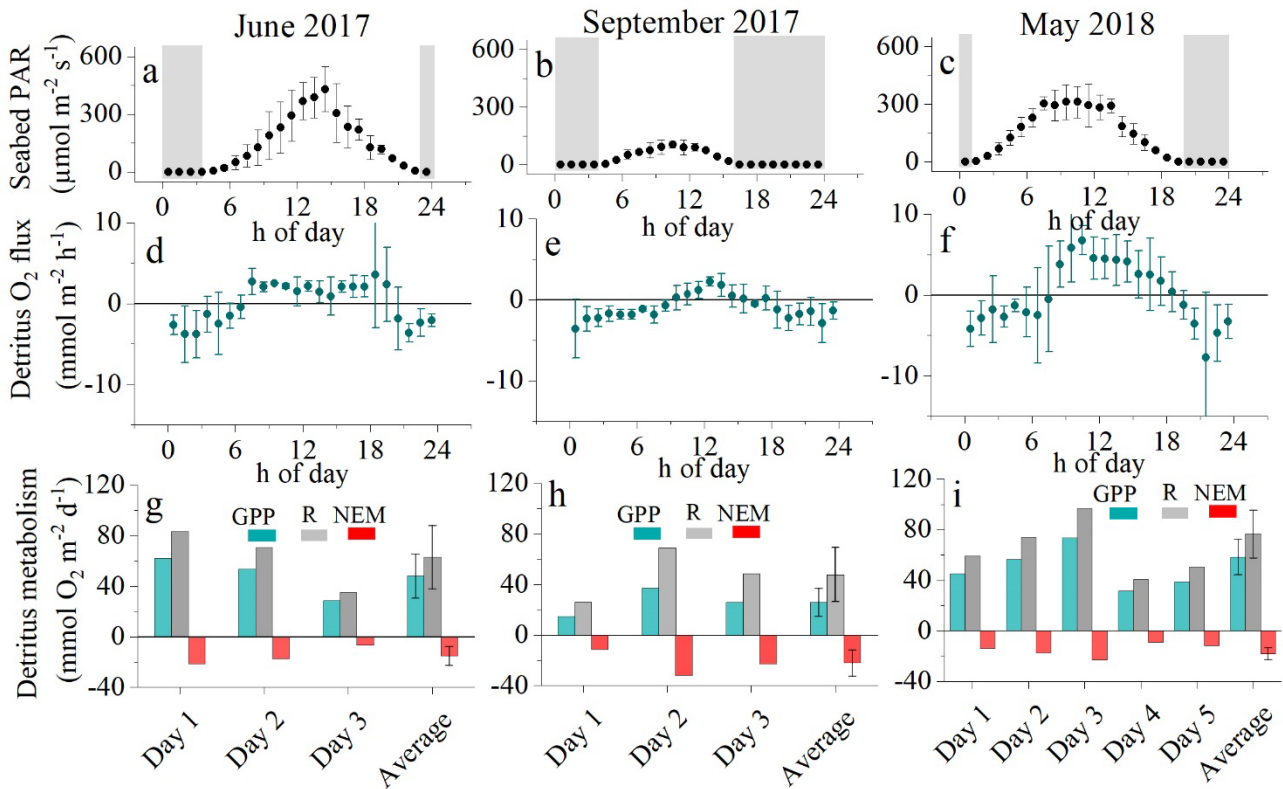
Fig. 4: Hourly seabed PAR (a, b, c) with night-time periods grey shaded, hourly O_2 fluxes (d, e, f)

and daily metabolism estimates of gross primary production (GPP), respiration (R), and net

ecosystem metabolism (NEM) for the detritus canopy for the three measurement campaigns (g, h,

i). Seabed PAR and O_2 fluxes are shown as mean ± 1 s.d. and are binned by the hour of day.

There was a significant positive relationship between near-bed incident PAR and the benthic O_2

flux (Fig. 5). Light-saturation curves fitted to hourly data from all deployments indicated a

maximum gross primary production rate (P_m) of 5.14 ± 0.56 mmol O_2 m^{-2} h^{-1}, an α of 0.03 ± 0.01,

and a R rate of 1.92 ± 0.26 mmol O_2 m^{-2} h^{-1}. Light saturation (I_k) of the detritus canopy occurred at

irradiances greater than ~170 μmol PAR m^{-2} s^{-1}.
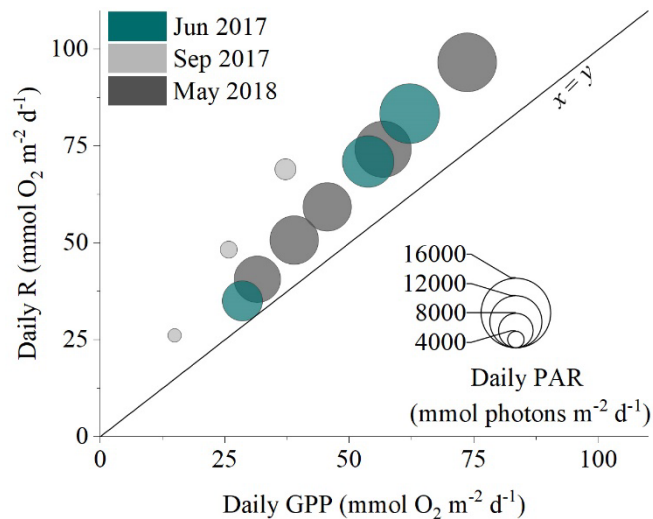
Fig. 5: The daily balance between detritus gross primary production (GPP) and respirati®(R) for the three measurement campaigns. Symbol size corresponds to the daily integrated PAR reaching the seafloor.
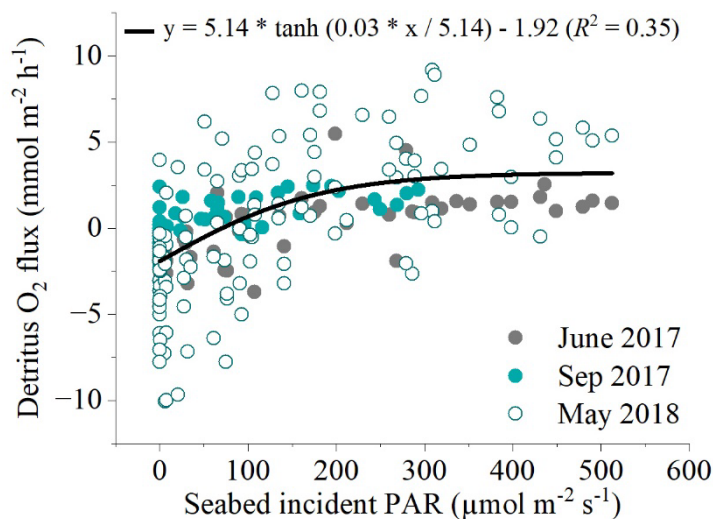
Fig. 6: Relationship between all hourly in situ benthic O_2 fluxes at the detritus site and light availability from the three flux datasets measured. A modified photosynthesis-irradiance curve by Platt et al. (1980) is shown as the line-of-best-fit to the global dataset.

3.5. Macrobenthic diversity and abundance

The detritus site had a biomass of accumulated macrophyte (*F. vesiculosus*) detritus of 1666 ± 223 g dry weight m^{-2} (mean $\pm$ SE, $n = 4$), approximately 1.5-fold larger than nearby intact *F. vesiculosus*

canopies (Table 2). Detritus accumulation in the five other habitats was around 100-fold smaller. The area of the detritus site estimated using Google Earth was 2300 m^2, amounting to 3,800 kg dry weight of *F. vesiculosus* fragments. Macrofauna abundance ranged from 2700 ± 900 ind. m^{-2} at the bare sediments site to 17300 ± 2400 ind. m^{-2} at the sheltered *F. vesiculosus* site (mean $\pm$ SE, $n = 4$) (Table 3). Macrofauna biomass ranged from 6 ± 2 g m^{-2} at the bare site to 41 ± 9 g m^{-2} at the exposed seagrass site (mean $\pm$ SE, $n = 4$), and the number of species ranged from 6 to 23, with the lowest values measured at the bare sediments and detritus sites, and the highest values at the sheltered *F. vesiculosus* site (Table 3).

At the detritus site, there was a low abundance of epifaunal crustaceans when compared to other habitats with canopies. Key species, such as the amphipod *Gammarus spp.* were notably absent, and isopods such as *Idotea spp.* were present in low abundance (Table A3). Similarly, there was a notable absence of bivalves such as the soft-shelled clam, *Mya arenaria*, and the cockle *Cerastoderma glaucum*. Polychaetes such as *Hediste diversicolor* and *Marenzelleria spp.* were also absent from the detritus site but present in other sedimentary habitats (Table A3). The nMDS ordination of the macrofaunal assemblages indicated a clear separation of points representing the different habitat sites (ANOSIM: $R^2 = 0.865$; $p < 0.001$). The assemblages from the bare sand and the detritus sites formed separated site groupings compared to the vegetated sites ('*Fucus*' and 'seagrass', both exposed and sheltered). Within the vegetated sites, the assemblages of the 'seagrass sheltered' and the '*Fucus* sheltered' sites were the most different (Fig. 7).

Table 2: Vegetation abundance and biomass (dry weight) at the six study sites. Abundance is shoots per m^2 for seagrass and individuals per m^2 for *F. vesiculosus*. Values are mean ± SE.

Site	Abundance per m^2	Above-ground biomass (g m^{-2})	Belowground biomass (g m^{-2})	Detritus (g m^{-2})	Biomass other species (g m^{-2})
Macrophyte detritus	-	-	-	1666 ± 223	-
Bare sediments	-	-	-	-	-
Sheltered *Z. marina*	768 ± 92	21 ± 2	8 ± 1	58 ± 13	0.1 ± 0.1
Exposed *Z. marina*	2565 ± 164	69 ± 7	25 ± 3	16 ± 2	0.2 ± 0.2
Sheltered *F. vesiculosus*	16 ± 2	1244 ± 58	-	55 ± 11	-
Exposed *F. vesiculosus*	16 ± 2	1112 ± 119	-	20 ± 2	-

Table 3: Macrofauna abundance, biomass (ash-free dry weight), and number of species at the six study sites.

Site	Infauna abundance (ind. m^{-2})	Epifauna abundance (ind. m^{-2})	Total abundance (ind. m^{-2})	Infauna biomass (g m^{-2})	Epifauna biomass (g m^{-2})	Total biomass (g m^{-2})	Number of species
Macrophyte detritus	4175 ± 2885	493 ± 37	4668 ± 2885	5 ± 3	5 ± 0	9 ± 3	6
Bare sediments	2719 ± 854	-	2719 ± 854	6 ± 2	-	6 ± 2	6
Sheltered *Z. marina*	6110 ± 787	3020 ± 874	9130 ± 1176	30 ± 6	2 ± 0	33 ± 6	18
Exposed *Z. marina*	6959 ± 620	3316 ± 772	10275 ± 990	31 ± 8	10 ± 2	41 ± 9	16
Sheltered *F. vesiculosus*	-	17259 ± 2421	17259 ± 2421	-	11 ± 2	11 ± 2	23
Exposed *F. vesiculosus*	-	3551 ± 609	3551 ± 609	-	7 ± 2	7 ± 2	12
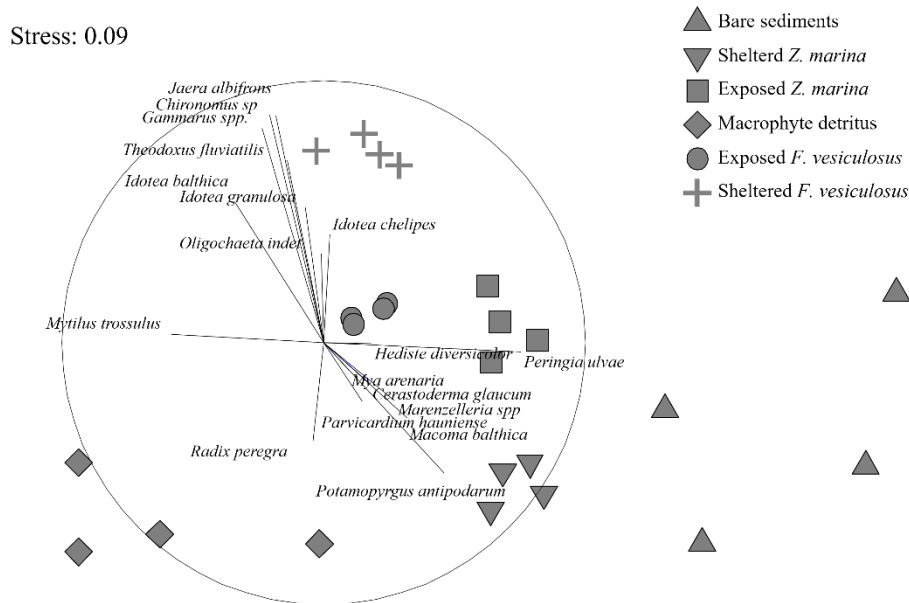
Fig. 7: A non-metric multidimensional scaling (nMDS) ordination of the macrofaunal assemblages indicated a clear separation of points representing the different habitat sites. The assemblages from the bare sand and the detritus sites formed separate site groupings compared to the vegetated sites. Data from May 2018 (see Table 1).

4. Discussion

4.1. Detritus metabolism

The eddy covariance measurements document a highly active detrital canopy that photosynthesized as well as respired. High daily rates of GPP of up to 75 mmol O_2 m^{-2} d^{-1} and R of 100 mmol O_2 m^{-2} d^{-1} are comparable to some of the most productive habitats in the area, such as dense seagrass meadows (*Zostera marina*) and intact canopies of bladder wrack (*Fucus vesiculosus*) (Attard et al., 2019b). However, intact canopies of *F. vesiculosus* function very differently to detritus canopies from a metabolic standpoint. In June 2017, two eddy covariance instruments were deployed in parallel: one at the detritus site, and another at a nearby intact canopy. While the detritus was net heterotrophic (NEM = -15 mmol O_2 m^{-2} d^{-1}; GPP:R = 0.76), the intact *F. vesiculosus* canopy was strongly net autotrophic (NEM = 167 mmol O_2 m^{-2} d^{-1}; GPP:R = 6.40) (Attard et al., 2019b). Daily R at the detritus site was up to ~5-fold larger than that at a nearby (within 4 km) site with bare sediments and up to twice as high as a neighbouring intact canopy of *F. vesiculosus* (Attard et al., 2019b). Decaying (and respiring) fragments of *F. vesiculosus* could contribute substantially to the O_2 uptake rate: laboratory incubations of *F. vesiculosus* fragments resolved respiration rates ~5

μmol O_2 g dw^{-1} h^{-1}, equivalent to ~25 mmol O_2 m^{-2} d^{-1} when upscaled to *in situ* biomass observed at the detritus site (data not shown).

Notwithstanding the key metabolic differences between detritus and other neighbouring sites, the flux measurements (Figure 4) indicate that shallow detritus accumulation zones are not just regions of organic matter remineralization, but rather they synthesize substantial amounts of organic matter through primary production. The range in daily GPP:R from 0.53 to 0.81 indicates that primary production can offset a substantial proportion of the respiratory demand, which extends the persistence of detritus in the coastal zone. These observations are consistent with the laboratory study by Frontier et al. (2021), who determined that following detachment, kelp (*Laminaria hyperborea* and *L. ochroleuca*) fragments retain physiological and reproductive capabilities for up to several months. Carbon retention within the coastal zone and export to deeper, sedimentary accumulation regions would therefore be larger than would be predicted by decomposition theory alone. Similarly, slow, and incomplete degradation of algae detritus under low [O_2] conditions, which could occur, for instance, in the bottom layers of detrital canopies or in the large anoxic basins of the Baltic Sea (Conley et al., 2009), would increase carbon retention, transfer, and sequestration potential (Pedersen et al., 2021).

4.2. Periodic benthic hypoxia

Our in situ measurements performed over a few days in late spring document that subtidal detritus accumulation zones uniquely experience dynamic [O_2] conditions driven by sunlight availability and flow velocity, with rapid [O_2] oscillations and frequent periods of hypoxia (Table 1). Hypoxic conditions were largely restricted to the lower ~5 cm of the canopy and were only revealed by sensors placed directly above the sediment surface (< 5 cm distance). At the onset of wave-driven mixing, hypoxic waters from within the canopy propagated upwards into the water column and were registered by fast-response [O_2] sensors located 10 cm above the canopy (~35 cm above the seafloor). This observation suggests that the [O_2] conditions inside the entire canopy and even in the water column directly above can reach hypoxic conditions for a few minutes (Fig. 3). Such pulses, however, were not registered by the slow-response [O_2] optodes with a factory-specified T$_{90}$ < 2 min. The minimum [O_2] observed by these sensors placed at 10 cm and 35 cm above the seafloor was 158 and 229 μmol L^{-1}, respectively, and thus well above hypoxic conditions.

The importance of measuring [O_2] close to the seafloor was demonstrated more than 40 years ago by Jorgensen (1980), and since then, other researchers have investigated the distribution of

412   dissolved constituents such as O_2 and nutrients in the benthic boundary layer (Holtappels et al.,

413   2011). These studies document that solute gradients are largest near the seafloor. For practical

414   reasons, however, coastal monitoring programs measure $[O_2]$ further away from the seafloor.

415   Models based on monitoring data suggest that hypoxia is prevalent in only small areas of the

416   shallow subtidal zone. For instance, models for the northern Baltic Sea, which cover a total seabed

417   area of 12435 km^2 of which 2211 km^2 is in shallow waters <5 m depth, indicate that just 16.5 km^2

418   (or 0.75% of shallow waters) are prone to hypoxia (Virtanen et al., 2019). Given that large

419   quantities of drifting macrophytes are a common phenomenon in the shallow subtidal zone of the

420   northern Baltic Sea (Norkko and Bonsdorff, 1996a), it is likely that coastal hypoxia is currently

421   underestimated because large-scale models are largely based on measurements performed higher

422   above the seafloor (0.5-1.0 m) (Virtanen et al., 2019; Conley et al., 2011).

4.3. Biodiversity and [O_2] dynamics in detritus canopies

424   Despite being considered a temporary habitat, detritus was found in abundance at our study site on

425   all occasions in May, June, and September. This type of habitat is likely quite widespread in the

426   Baltic. Habitat distribution models for the area indicate a dominance of *F. vesiculosus* canopies in

427   shallow waters < 5 m depth (Virtanen et al., 2018), and these canopies are expected to export

428   substantial amounts of organic matter (~0.3 kg C m^{-2} yr^{-1}) which can accumulate in topographical

429   depressions with limited water exchange (Attard et al., 2019a). Topographic depressions occupy

430   ~1350 km^2 or ~11% of the northern Baltic Sea (Virtanen et al., 2019). During a recent seasonal

431   study, we observed the highest abundance of detritus at our study site in summer and autumn,

432   coinciding with high southerly winds that erode intact canopies in shallower waters (Attard et al.,

433   2019a). However, we also observed significant canopy erosion in winter when a substantial biomass

434   of *F. vesiculosus* froze into sea ice and got dislodged once the ice broke up (Fig. 7). Therefore,

435   some degree of drifting detritus might be common throughout the year. Drifting detritus constitutes

436   a significant habitat structure. Given high enough biomass, however, detritus canopies can be a

437   challenging habitat for most species. At our study site, hypoxic conditions uniquely occurred at the

438   detritus site and for around a quarter of the deployment time (Table 1). We can expect these

439   conditions to be particularly challenging for crustaceans, the most hypoxia-sensitive

440   macroinvertebrate group (Vaquer-Sunyer and Duarte, 2008). Indeed, we only found one crustacean

441   species at this site- the isopod *Idotea balthica* (Table A3)- which is mobile and can tolerate hypoxic

442   conditions for a few hours (Vetter and Dayton, 1999). All other invertebrates observed at the

443   detritus site were mollusks (Table A3), the most hypoxia-tolerant marine invertebrate group

444 (Vaquer-Sunyer and Duarte, 2008). Other tolerant species include the blue mussel *Mytilus trossulus*

445 *x edulis* that can survive > 300 h of anoxia (Jorgensen, 1980), although the survival of larvae

446 depends on its developmental stage (Diaz and Rosenberg, 1995). Similarly, the mudsnail

447 *Peringia ulvae* is highly mobile and can survive > 150 h of anoxia (Jorgensen, 1980; Norkko et al.,

448 2000).

449 Overall, the dynamic $[O_2]$ conditions in detrital canopies seem to be challenging for most species in

450 this region of the Baltic Sea, with lethal and non-lethal thresholds frequently being exceeded on

451 timescales of hours to days. We currently have a poor understanding of the extent of periodic

452 hypoxia in coastal waters, because $[O_2]$ measurements are performed at some distance away from

453 the seabed. While this is a practical approach that is done to minimize sensor fouling and damage, it

454 does not reveal the full extent of coastal hypoxia. If implemented widely, sensor arrays, as

455 described herein, and sensor elevators (e.g. (Holtappels et al., 2011)) can fill in this knowledge gap

456 and provide important insights into the ecological status and biogeochemical cycling that is needed

457 for the sustainable management of coastal ecosystems.

458

459 Fig. 8: substantial detritus accumulation was observed in late winter (March 2021) when *F.*

460 *vesiculosus* froze into sea ice and got dislodged once the ice broke up. (Photo by Alf Norkko)

Author contribution

All authors contributed significantly to designing the research, funding the study, collecting the data, analyzing samples and data, and interpreting the results. KMA wrote the paper with input from all authors.

Competing interests

The authors declare that they have no conflict of interest.

Data availability

All data presented in this paper will be made available in a FAIR-aligned data repository.

Acknowledgements

Colleagues at the Tvärminne Zoological Station provided valuable assistance with fieldwork and logistics. Anni Glud at the University of Southern Denmark constructed the oxygen microsensors used in this study. Elina Virtanen at the Finnish Environmental Institute (SYKE) provided spatial data used to estimate the potential extent of detritus canopies. The Walter and Andrée de Nottbeck Foundation supported this work through a postdoctoral fellowship to KMA and through a Masters fellowship to AL. Further funding for this project was provided by research grants from the Academy of Finland (project ID 294853), the University of Helsinki and Stockholm University strategic fund for collaborative research (the Baltic Bridge initiative), and Denmark's Independent Research Fund (project ID 7014-00078). This study has utilized research infrastructure facilities provided by FINMARI (Finnish Marine Research Infrastructure network, The Academy of Finland, project ID 283417).

References

Attard, K. M. and Glud, R. N.: Technical Note: Estimating light-use efficiency of benthic habitats using underwater O-2 eddy covariance, Biogeosciences, 17, 4343-4353, 2020.

Attard, K. M., Rodil, I. F., Berg, P., Norkko, J., Norkko, A., and Glud, R. N.: Seasonal metabolism and carbon export potential of a key coastal habitat: The perennial canopy-forming macroalga *Fucus vesiculosus*, Limnol Oceanogr, 64, 149-164, 10.1002/lno.11026, 2019a.

Attard, K. M., Rodil, I. F., Glud, R. N., Berg, P., Norkko, J., and Norkko, A.: Seasonal ecosystem metabolism across shallow benthic habitats measured by aquatic eddy covariance, Limnology and Oceanography Letters, 4, 79-86, 10.1002/lol2.10107, 2019b.

Berg, P. and Pace, M. L.: Continuous measurement of air-water gas exchange by underwater eddy covariance, Biogeosciences, 14, 5595-5606, 2017.

Berg, P., Røy, H., and Wiberg, P. L.: Eddy correlation flux measurements: the sediment surface area that contributes to the flux, Limnol Oceanogr, 52, 1672-1684, 10.4319/lo.2007.52.4.1672, 2007.

Berg, P., Huettel, M., Glud, R. N., Reimers, C. E., and Attard, K. M.: Aquatic Eddy Covariance: The Method and Its Contributions to Defining Oxygen and Carbon Fluxes in Marine Environments, Annual Review of Marine Science, 14, 431-455, 10.1146/annurev-marine-042121-012329, 2022.

Berg, P., Røy, H., Janssen, F., Meyer, V., Jorgensen, B. B., Huettel, M., and de Beer, D.: Oxygen uptake by aquatic sediments measured with a novel non-invasive eddy-correlation technique, Marine Ecology Progress Series, 261, 75-83, 10.3354/Meps261075, 2003.

Bittig, H. C., Kortzinger, A., Neill, C., van Ooijen, E., Plant, J. N., Hahn, J., Johnson, K. S., Yang, B., and Emerson, S. R.: Oxygen Optode Sensors: Principle, Characterization, Calibration, and Application in the Ocean, Frontiers in Marine Science, 4, 2018.

Breitburg, D., Levin, L. A., Oschlies, A., Gregoire, M., Chavez, F. P., Conley, D. J., Garcon, V., Gilbert, D., Gutierrez, D., Isensee, K., Jacinto, G. S., Limburg, K. E., Montes, I., Naqvi, S. W. A., Pitcher, G. C., Rabalais, N. N., Roman, M. R., Rose, K. A., Seibel, B. A., Telszewski, M., Yasuhara, M., and Zhang, J.: Declining oxygen in the global ocean and coastal waters, Science, 359, 46-+, 2018.

Broch, O. J., Hancke, K., and Ellingsen, I. H.: Dispersal and Deposition of Detritus From Kelp Cultivation, Frontiers in Marine Science, 9, 2022.

Broch, O. J., Alver, M. O., Bekkby, T., Gundersen, H., Forbord, S., Handa, A., Skjermo, J., and Hancke, K.: The Kelp Cultivation Potential in Coastal and Offshore Regions of Norway, Frontiers in Marine Science, 5, 2019.

Camillini, N., Attard, K. M., Eyre, B. D., and Glud, R. N.: Resolving community metabolism of eelgrass Zostera marina meadows by benthic flume-chambers and eddy covariance in dynamic coastal environments, Marine Ecology Progress Series, 661, 97-114, 2021.

Carstensen, J. and Conley, D. J.: Baltic Sea Hypoxia Takes Many Shapes and Sizes, Limnology and Oceanography Bulletin, 28, 125-129, https://doi.org/10.1002/lob.10350, 2019.

Conley, D. J., Carstensen, J., Aigars, J., Axe, P., Bonsdorff, E., Eremina, T., Haahti, B. M., Humborg, C., Jonsson, P., Kotta, J., Lannegren, C., Larsson, U., Maximov, A., Medina, M. R., Lysiak-Pastuszak, E., Remeikaite-Nikiene, N., Walve, J., Wilhelms, S., and Zillen, L.: Hypoxia Is Increasing in the Coastal Zone of the Baltic Sea, Environ Sci Technol, 45, 6777-6783, 10.1021/es201212r, 2011.

Conley, D. J., Bjorck, S., Bonsdorff, E., Carstensen, J., Destouni, G., Gustafsson, B. G., Hietanen, S., Kortekaas, M., Kuosa, H., Meier, H. E. M., Muller-Karulis, B., Nordberg, K., Norkko, A., Nurnberg, G., Pitkanen, H., Rabalais, N. N., Rosenberg, R., Savchuk, O. P., Slomp, C. P., Voss, M., Wulff, F., and Zillen, L.: Hypoxia-Related Processes in the Baltic Sea, Environ Sci Technol, 43, 3412-3420, 10.1021/es802762a, 2009.

Davanzo, C. and Kremer, J. N.: Diel Oxygen Dynamics and Anoxic Events in an Eutrophic Estuary of Waquoit Bay, Massachusetts, Estuaries, 17, 131-139, 1994.

Diaz, R. J. and Rosenberg, R.: Marine benthic hypoxia: A review of its ecological effects and the behavioural responses of benthic macrofauna, Oceanography and Marine Biology - an Annual Review, Vol 33, 33, 245-303, 1995.

Diaz, R. J. and Rosenberg, R.: Spreading dead zones and consequences for marine ecosystems, Science, 321, 926-929, 10.1126/science.1156401, 2008.

531 Duarte, C. M. and Cebrián, J.: The fate of marine autotrophic production, Limnol Oceanogr, 41, 1758-1766,
532 DOI 10.4319/lo.1996.41.8.1758, 1996.
533 Fenchel, T. and Glud, R. N.: Benthic primary production and O2-CO2 dynamics in a shallow-water sediment:
534 Spatial and temporal heterogeneity, Ophelia, 53, 159-171, 2000.
535 Frontier, N., de Bettignies, F., Foggo, A., and Davoult, D.: Sustained productivity and respiration of
536 degrading kelp detritus in the shallow benthos: Detached or broken, but not dead, Mar Environ Res, 166,
537 2021.
538 Garcia, H. E. and Gordon, L. I.: Oxygen Solubility in Seawater - Better Fitting Equations, Limnol Oceanogr,
539 37, 1307-1312, 1992.
540 Glud, R. N.: Oxygen dynamics of marine sediments, Mar Biol Res, 4, 243-289, 2008.
541 Glud, R. N., Rysgaard, S., Fenchel, T., and Nielsen, P. H.: A conspicuous H2S-oxidizing microbial mat from a
542 high-latitude Arctic fjord (Young Sound, NE Greenland), Mar Biol, 145, 51-60, DOI 10.1007/s00227-004-
543 1296-8, 2004.
544 Hansen, J. C. R. and Reidenbach, M. A.: Turbulent mixing and fluid transport within Florida Bay seagrass
545 meadows, Adv Water Resour, 108, 205-215, 2017.
546 Holtappels, M., Kuypers, M. M. M., Schluter, M., and Bruchert, V.: Measurement and interpretation of
547 solute concentration gradients in the benthic boundary layer, Limnol Oceanogr-Meth, 9, 1-13, 2011.
548 Jorgensen, B. B.: Seasonal Oxygen Depletion in the Bottom Waters of a Danish Fjord and Its Effect on the
549 Benthic Community, Oikos, 34, 68-76, 1980.
550 Juska, I. and Berg, P.: Variation in seagrass meadow respiration measured by aquatic eddy covariance,
551 Limnology and Oceanography Letters, 7, 410-418, https://doi.org/10.1002/lol2.10276, 2022.
552 Krumhansl, K. A. and Scheibling, R. E.: Production and fate of kelp detritus, Marine Ecology Progress Series,
553 467, 281-302, 10.3354/meps09940, 2012.
554 Long, M. H. and Nicholson, D. P.: Surface gas exchange determined from an aquatic eddy covariance
555 floating platform, Limnol Oceanogr-Meth, 16, 145-159, 2018.
556 McGinnis, D. F., Cherednichenko, S., Sommer, S., Berg, P., Rovelli, L., Schwarz, R., Glud, R. N., and Linke, P.:
557 Simple, robust eddy correlation amplifier for aquatic dissolved oxygen and hydrogen sulfide flux
558 measurements, Limnol Oceanogr-Meth, 9, 340-347, DOI 10.4319/lom.2011.9.340, 2011.
559 Middelburg, J. J. and Levin, L. A.: Coastal hypoxia and sediment biogeochemistry, Biogeosciences, 6, 1273-
560 1293, DOI 10.5194/bg-6-1273-2009, 2009.
561 Norkko, A. and Bonsdorff, E.: Population responses of coastal zoobenthos to stress induced by drifting algal
562 mats, Marine Ecology Progress Series, 140, 141-151, DOI 10.3354/meps140141, 1996a.
563 Norkko, A. and Bonsdorff, E.: Rapid zoobenthic community responses to accumulations of drifting algae,
564 Marine Ecology Progress Series, 131, 143-157, DOI 10.3354/meps131143, 1996b.
565 Norkko, A., Villnas, A., Norkko, J., Valanko, S., and Pilditch, C.: Size matters: implications of the loss of large
566 individuals for ecosystem function, Sci Rep-Uk, 3, ARTN 2646

567 10.1038/srep02646, 2013.
568 Norkko, J., Bonsdorff, E., and Norkko, A.: Drifting algal mats as an alternative habitat for benthic
569 invertebrates: Species specific responses to a transient resource, Journal of Experimental Marine Biology
570 and Ecology, 248, 79-104, 2000.
571 Pedersen, M. F., Filbee-Dexter, K., Frisk, N. L., Sarossy, Z., and Wernberg, T.: Carbon sequestration potential
572 increased by incomplete anaerobic decomposition of kelp detritus, Marine Ecology Progress Series, 660, 53-
573 67, 2021.
574 Platt, T., Gallegos, C. L., and Harrison, W. G.: Photoinhibition of photosynthesis in natural assemblages of
575 marine phytoplankton, J Mar Res, 38, 687-701, 1980.
576 Rheuban, J. E., Berg, P., and McGlathery, K. J.: Multiple timescale processes drive ecosystem metabolism in
577 eelgrass (*Zostera marina*) meadows, Marine Ecology Progress Series, 507, 1-13, 10.3354/meps10843, 2014.

578 Robertson, E. K., Roberts, K. L., Burdorf, L. D. W., Cook, P., and Thamdrup, B.: Dissimilatory nitrate reduction
579 to ammonium coupled to Fe(II) oxidation in sediments of a periodically hypoxic estuary, Limnol Oceanogr,
580 61, 365-381, 2016.
581 Rodil, I. F., Attard, K. M., Norkko, J., Glud, R. N., and Norkko, A.: Towards a sampling design for
582 characterizing habitat-specific benthic biodiversity related to oxygen flux dynamics using Aquatic Eddy
583 Covariance, Plos One, 14, e0211673, 10.1371/journal.pone.0211673, 2019.
584 Rumohr, H., Brey, T., and Ankar, S.: A compilation of biometric conversion factors for benthic invertebrates
585 of the Baltic Sea, Baltic Marine Biologists, 9, 1-56, 1987.
586 Smith, S. V.: Marine macrophytes as a global carbon sink, Science, 211, 838-840, DOI
587 10.1126/science.211.4484.838, 1981.
588 Tyler, R. M., Brady, D. C., and Targett, T. E.: Temporal and Spatial Dynamics of Diel-Cycling Hypoxia in
589 Estuarine Tributaries, Estuar Coast, 32, 123-145, 10.1007/s12237-008-9108-x, 2009.
590 Vaquer-Sunyer, R. and Duarte, C. M.: Thresholds of hypoxia for marine biodiversity, P Natl Acad Sci USA,
591 105, 15452-15457, 10.1073/pnas.0803833105, 2008.
592 Vetter, E. W. and Dayton, P. K.: Organic enrichment by macrophyte detritus, and abundance patterns of
593 megafaunal populations in submarine canyons, Marine Ecology Progress Series, 186, 137-148, 1999.
594 Virtanen, E., Viitasalo, M., Lappalainen, J., and Moilanen, A.: Evaluation, gap analysis, and potential
595 expansion of the Finnish marine protected area network, Frontiers in Marine Science,
596 10.3389/fmars.2018.00402, 2018.
597 Virtanen, E. A., Norkko, A., Sandman, A. N., and Viitasalo, M.: Identifying areas prone to coastal hypoxia -
598 the role of topography, Biogeosciences, 16, 3183-3195, 2019.
599